CEAS-GNC-2022-012

CEAS EuroGNC 2022
"Conference on Guidance, Navigation and Control"
3-5 May 2022 @ Technische Universität Berlin, Germany

System Identification of a Nonlinear UAV Model with Distributed Aerodynamics and Flexible Structure

Benjamin Herrmann Research Engineer, Institute of Aircraft Systems Engineering, Hamburg University of Technology, Nesspriel 5, 21129 Hamburg, Germany. benjamin.herrmann@tuhh.de

Julian Theis Lecturer, Institute of Aircraft Systems Engineering, Hamburg University of Technology, Nesspriel 5, 21129 Hamburg, Germany. julian.theis@tuhh.de

Frank Thielecke Professor, Institute of Aircraft Systems Engineering, Hamburg University of Technology, Nesspriel 5, 21129 Hamburg, Germany. frank.thielecke@tuhh.de

ABSTRACT

This paper presents the nonlinear system identification of a slightly flexible 25kg fixed-wing UAV in the time domain using a computationally efficient distributed aerodynamics model and a linear structural dynamics representation. The equations of motion are formed by making use of the free vibration modes of the structure and the mean axis formulation. The structural modes and mode shapes are determined from ground vibration tests. The distributed aerodynamics, accounting for elastic deformations, are modeled using a quasi-steady stability and control derivative approach and by applying strip theory. Initial distributions for the derivatives are obtained from vortex-lattice-method calculations. For matching the model response to the measured response, parameters for scaling the initial derivative distributions are introduced. The flexible model is subsequently identified based on flight test data using the output error method in the time domain and maximum likelihood estimation. A good overall identification result is achieved with a close match of the fast aircraft dynamics. Lastly, an evaluation is given on the suitability of the identified model for real-time simulation, loads estimation and active load control law design.

Keywords: System Identification; Nonlinear Flexible Aircraft Modeling; UAV

Nomenclature

a_x, a_y, a_z	=	Accelerations (longitundinal, lateral, vertical) expressed in O_{B^R} coordinates, m/s^2
$\boldsymbol{b}, \boldsymbol{b}_r$	=	Deformed and undeformed position vector relative to O_{B^G}, m
c_i	=	Local strip chord, m
$\overline{c}$	=	Wing aerodynamic mean chord, m
cm	=	Center of mass
$\boldsymbol{C}^F$	=	Coefficient vector of aerodynamic forces
$\boldsymbol{C}^M$	=	Coefficient vector of aerodynamic moments
$\boldsymbol{d}$	=	Elastic deformation vector in O_{B^R} coordinates, m
dV	=	Volume element, m^3
dy	=	Local strip width, m
$\boldsymbol{F}^{ext}$	=	Vector of external forces, N

$\boldsymbol{F}^A$	=	Vector of aerodynamic forces, N
$\boldsymbol{G}$	=	Gravity acceleration vector in O_I coordinates, m/s^2
h	=	Altitude, m
J	=	Inertia tensor, kg·m^2
k	=	Factor of induced drag term
m	=	Aircraft mass, kg
$\boldsymbol{M}^A$	=	Vector of aerodynamic moments, N·m
$\boldsymbol{M}^{ext}$	=	Vector of external moments, N·m
n_e	=	Number of elastic modes
n_s	=	Number of strips
O_{A^S}	=	Local aerodynamic strip frame
O_{B^G}	=	Global body-fixed frame
O_{B^R}	=	Body-reference frame (center of mass)
O_{B^S}	=	Local strip-fixed frame
O_I	=	Inertial reference frame
$\boldsymbol{p}$	=	Position vector of mass element relative to O_{B^R}, m
p, q, r	=	Angular rates (roll, pitch, yaw), rad/s
p_s	=	Static pressure, Pa
$\overline{q}$	=	Dynamic pressure, Pa
$\overline{q}_A$	=	Dynamic pressure of local relative flow, Pa
$\overline{q}_N$	=	Dynamic pressure of local normal flow, Pa
Q_{η_j}	=	Generalized forces of j-th mode, N·m
$\boldsymbol{r}$	=	Position vector of mass element relative to O_I, m
$\boldsymbol{r}_0$	=	Position vector of origin of O_{B^R}, m
$\overline{s}$	=	Half wing span, m
$\boldsymbol{s}$	=	Undeformed position vector relative to O_{B^R}, m
S_i	=	Local strip surface area, m^2
S_{ref}	=	Wing reference surface area, m^2
T	=	Air temperature, deg
$\boldsymbol{T}_{B^R I}$	=	Transformation matrix from O_I to O_{B^R}
u, v, w	=	Translational velocities (longitudinal, lateral, vertical) expressed in O_{B^R} coordinates, m/s
u_g, v_g, w_g	=	Translational velocities (longitudinal, lateral, vertical) expressed in O_I coordinates, m/s
u_A, v_A, w_A	=	Translational aerodynamic velocities (longitudinal, lateral, vertical), m/s
V_A	=	Aerodynamic velocity at O_{B^R}, m/s
$\boldsymbol{V}_{A,i}$	=	Local aerodynamic velocity vector, m/s
$\boldsymbol{V}_{N,i}$	=	Local normal flow vector, m/s
V_{TAS}	=	True airspeed, m/s
X_0	=	Steady flow-separation point on the upper surface
α	=	Angle of attack at O_{B^R}, rad
$\alpha_{\text{eff},i}$	=	Local strip effective angle of attack, rad
β	=	Angle of sideslip at O_{B^R}, rad
$\beta_{\text{eff},i}$	=	Local strip effective angle of sideslip, rad
δ_a	=	Aileron deflection, rad
δ_c	=	Control surface deflection, rad
δ_e	=	Elevator deflection, rad
δ_f	=	Flaperon deflection, rad
δ_r	=	Rudder deflection, rad
ε_b	=	Bending strain, 0.01%
ε_s	=	Shear strain, 0.01%
ε_t	=	Torsion strain, 0.01%

ε_T = Induced downwash angle, rad
$\varepsilon_0, \varepsilon_e$ = Rigid and elastic twist angle, rad
η = Generalized displacement coordinate
λ = Latitude, deg
μ = Generalized mass, kg·m^2
ν_0, ν_e = Rigid and elastic dihedral angle, rad
ω = Angular velocity vector of O_{B^R}, rad/s
ω_n = Undamped natural (modal) frequency, rad/s
ω_A = Aerodynamic angular velocity vector of O_{B^R}, rad/s
ρ = Air density, kg·m^{-3}
ξ = Structural (modal) damping ratio
φ = Longitude, deg
φ_e = Elastic sweep angle, rad
φ_{25c} = Rigid sweep angle at quarter chord line, rad
Φ, Θ, Ψ = Euler angles (roll, pitch, yaw), rad
Φ_d = Elastic translational displacement vector, m
Φ_j = Mode shape of j-th mode
Φ_φ = Elastic angular rotation vector, rad
Θ_i = Estimation parameter
$(\cdot)|_{B^R}$ = $(\cdot)$ expressed in O_{B^R}

1 Introduction

Main drivers in aircraft development relate to the need of an increased fuel efficiency to reduce operational cost and fulfill increasingly demanding environmental regulations. The efforts have led to constructing aircraft with lighter structures and higher aspect ratio wings which thus become more flexible. Due to the increase in flexibility, such wings are characterized by lower natural frequencies and exhibit increased in-flight deformations. These can lead to a coupling of rigid-body motion and elastic deformation through the aerodynamic forces and moments. Flight control systems further complicate the interaction, possibly leading to degraded [1] or unstable [2] control performance. Therefore, these interactions need to be considered in the design models for flight control systems.
Depending on the characteristics of the aircraft, the purpose of application, or the availability of experimental data, different modeling frameworks are required. In the context of this work, the objective is the development of an aeroelastic model for a slightly flexible 25kg fixed-wing UAV that can be adapted based on flight test data using system identification techniques in the time domain. The model is intended for real-time simulation, loads estimation, and active load control law design. Therefore, a model of moderate complexity with a limited number of state variables is required. Beyond that, it is desired to maintain a distributed aerodynamics model such that local forces and moments can be calculated.

An overview of different aerodynamics modeling and system identification activities including applications for flexible aircraft is given in [3]. The modeling of flexible aircraft is suggested with an additional dynamic-pressure dependent part associated with each stability and control derivative of a classical model structure. However, this approach is only valid provided the rigid-body and structural frequencies are sufficiently separated. A unified framework for modeling flexible aircraft is presented in [4] and later in [5]. The equations of motion are derived by Lagrange's equation and the principle of virtual work. Further, they make use of a modal representation of the structure and the mean axis constraints to minimize inertial coupling between the rigid-body and elastic degrees of freedom (assuming small deformations). The nonlinear equations of motion of the flexible aircraft then simplify and are presented in terms of the nonlinear equations of the rigid-body motion and additional linear differential equations for the modal deflections of the structure. The equations are solely coupled by the aerodynamic

forces and moments. The modeling of aerodynamics is further proposed by a quasi-steady stability and control derivative approach and by applying strip theory. Strip theory is a simple method often found in models concerned with the investigation of wake vortex encounter, namely aerodynamic interaction models (AIM) [6–8]. In strip theory, the lifting surfaces of the aircraft are divided into spanwise strips. Each strip is then treated as a two-dimensional airfoil with its local geometric and aerodynamic characteristics. This approach allows for the resolution of local relative flow conditions and the resulting change in force and moment distributions. Outside aerodynamic interaction models, the application of strip theory is e.g. found in real-time full-envelope aerodynamic models for small UAVs [9]. The modeling methodology of [4] was further adopted in later works by various authors, in [10] together with quasi-steady strip aerodynamics, and in [11, 12] together with unsteady aerodynamics using modified strip theory [13, 14] and indicial functions [15, 16]. The work of [10, 11] both aimed at modeling only incremental aerodynamics due to elastic deformations, assuming the availability of a rigid-body flight mechanics and aerodynamics model. System identification techniques for flexible aircraft in combination with the framework of [4, 5] can be found in [17, 18] for the identification of a high performance glider. Though keeping the quasi-steady derivative approach for modeling the aerodynamic forces, moments, and generalized loads, the derivatives are not determined by applying strip theory, but directly estimated as parameters within the parameter estimation process. This modeling approach is a the straightforward extension of the traditional rigid-body approach to a flexible structure, which can be easily combined with system identification techniques. However, the distributed property of the aerodynamics model is lost. Other applications of system identification for flexible aircraft are found e.g in [19] for the in-flight identification of structural modes using an eigensystem realization algorithm (ERA).

Given the review on the literature, the framework of [4, 5] is a powerful method for modeling slightly flexible aircraft. Further, strip theory is simple but effective for modeling local aerodynamic forces and moments. The objective of this work is to maintain this strip aerodynamics model while allowing for the adaption of the model using system identification techniques in the time domain. The paper is structured as follows. Section 2 introduces the slightly flexible unmanned test aircraft G-Flights Dimona and summarizes the test activities that were performed. Section 3 describes the modeling of the test aircraft. Within this section, the equations of motion are developed using the free vibration modes of the structure and the mean axis formulation of [4]. Further, the modeling of quasi-steady strip aerodynamics is explained. Lastly, section 4 presents the identification and evaluation of the flexible model.

2 Unmanned Test Aircraft G-Flights Dimona

The slightly flexible test aircraft G-Flights Dimona, depicted in Figure 1, is an unmanned replica of the *HK36 Super Dimona* at a scale of 1:3. It is driven by an electrical motor with a maximum power of 4kW, has a total mass of 25kg and a length of 2.4m. The original wings of the aircraft have been replaced by custom spar, rib, and foil manufactured wings with increased span and flexibility. The total wingspan of the aircraft is 5.4m with a total wing surface area of 1.68m^2. The aircraft can either be controlled by a safety-pilot via remote control or by a flight control computer. It is equipped with a total of four control surfaces at the trailing edge of each wing: inner/outer ailerons and inner/outer flaperons, which are used for lateral-directional control and for load control. The aircraft further comprises a rudder for lateral-directional control and two elevators for longitudinal control and load control.

2.1 Test Instrumentation

The aircraft is equipped with the standard test instrumentation of a rigid-body aircraft and an additional test instrumentation distributed along the fuselage, wings, and empennage. The standard test instrumentation comprises several sensors, computers, and radio equipment. An industry-grade high-precision inertial navigation platform (INS) supported by dual-antennas is used for the measurement of GPS position, attitude, velocities, and accelerations. An increased position accuracy of 0.02m is achieved

Fig. 1 Test Aircraft G-Flights Dimona

with a third antenna on ground providing Differential GPS correction. Airspeed, angle of attack, angle of sideslip, static air pressure, and air temperature are measured by three air data systems (ADS). They each consist of a five-hole-probe with an additional inertial measurement unit (IMU) and temperature sensor for measurement correction. The airdata systems are located at the left (ADS1) and the right (ADS2) wing as well as at the vertical tail (ADS3). The air data systems were developed in-house and calibrated within wind tunnel experiments [20]. The standard test instrumentation is completed by a data recorder computer and separate real-time flight control computer. The flight control computer serves as the main host for GNC applications and issues control outputs to the servos. Further, it supports direct code deployment from MATLAB/SIMULINK. Data distribution between the sensors and computers is implemented via Ethernet-network and Controller Area Network (CAN). Table 1 lists the available measurement parameters of the standard test instrumentation.

Table 1 Standard measurement parameters

Name	Symbol	Unit	Name	Symbol	Unit
Latitude	φ	deg	Lateral velocity	v_g^{INS}	m/s
Longitude	λ	deg	Vertical velocity	w_g^{INS}	m/s
Altitude	h	m	Longitudinal acceleration	a_x^{INS}	m/s^2
Roll angle	Φ	rad	Lateral acceleration	a_y^{INS}	m/s^2
Pitch angle	Θ	rad	Vertical acceleration	a_z^{INS}	m/s^2
Heading	Ψ	rad	Angle of attack	$\alpha^{\mathrm{ADS1/2/3}}$	deg
Roll rate	p^{INS}	rad/s	Angle of sideslip	$\beta^{\mathrm{ADS1/2/3}}$	deg
Pitch rate	q^{INS}	rad/s	Static pressure	$p_s^{\mathrm{ADS1/2/3}}$	Pa
Yaw rate	r^{INS}	rad/s	Dynamic pressure	$\overline{q}^{\mathrm{ADS1/2/3}}$	Pa
Longitudinal velocity	u_g^{INS}	m/s	Air temperature	$T^{\mathrm{ADS1/2/3}}$	°C

The additional test instrumentation is distributed at various stations along the fuselage, wings, and empennage to measure structural dynamics and loads. It comprises several IMUs and strain gauges (shear, bending, torsion) which are concentrated in load measurement stations (LMS). Figure 2 displays the distribution of the sensors along the test aircraft. Since the measurement of loads and structural dynamics for wings and empannage is of prime importance, most sensors are located in these areas.

2.2 Ground Vibration Test and Modal Analysis

Considering the slight flexibility of the test aircraft, the assumption of linear structural dynamics is reasonable. Therefore, it was decided to represent the elastic deformation of the structure by a set of free vibration modes and mode shapes. To determine the structural modes of the aircraft, a ground vibration test (GVT) and experimental modal analysis was performed at the Technische Universität Berlin. Ham-

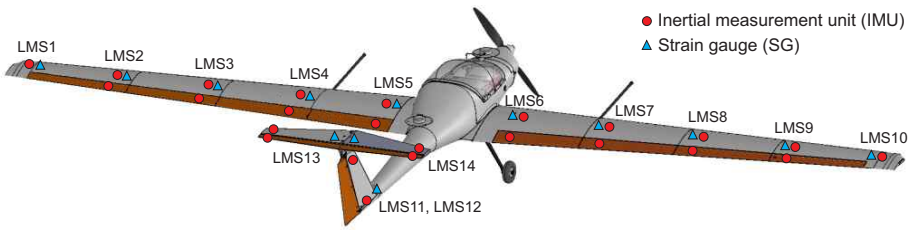

Fig. 2 Distribution of additional test instrumentation along the test aircraft

mer and shaker inputs were used to excite the structural vibrations of the aircraft. The first 7 structural modes up to the first symmetric wing torsion mode were identified and considered for the structural dynamics model. Details on the measurement setup, test execution, and results are presented in [21]. The structural mode shapes were subsequently determined from a finite element (FE) model adapted to the GVT data. Table 2 lists the 7 structural modes. Figure 3 further visualizes the modes. Especially the first symmetric wing bending mode exhibits a low natural frequency. Considering the servo actuator bandwidth of 6.74 Hz it is the mode likely to be excited by control action or atmospheric disturbance.

Table 2 First 7 identified structural modes of the G-Flights Dimona

Mode	Definition	Modal frequency ω_n (Hz)	Modal damping ξ (%)
1	First symmetric wing bending	3.97	0.85
2	First antisymmetric wing bending	8.56	1.38
3	First antisymmetric vertical tailplane bending	11.18	1.24
4	First symmetric in-plane wing bending	13.21	1.83
5	Second symmetric wing bending	14.60	1.79
6	First symmetric horizontal tailplane bending	17.24	2.76
7	First symmetric wing torsion	25.83	1.91

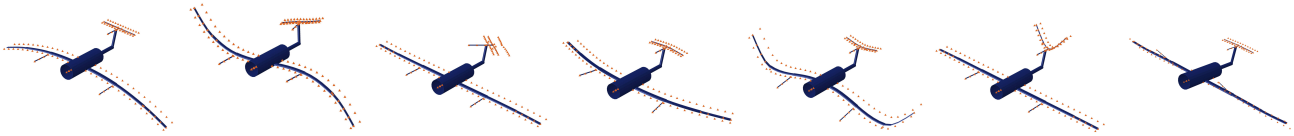

(a) Mode 1 **(b) Mode 2** **(c) Mode 3** **(d) Mode 4** **(e) Mode 5** **(f) Mode 6** **(g) Mode 7**

Fig. 3 Visualization of the first 7 structural modes of the G-Flights Dimona

2.3 Flight Tests

A comprehensive flight test campaign was performed to acquire flight data for system identification. The campaign included a total of 7 flights with 109 maneuvers performed. All maneuvers were executed with the help of an in-house developed autopilot for aerodynamic parameter identification [22], which was adapted based on an a priori estimation of the rigid-body dynamics. Details on the overall concept and main components of the test setup are given in [23]. A variety of classical maneuvers specifically designed for the identification of the rigid-body dynamics were flown [24]. They comprised multiple longitudinal maneuvers including 3-2-1-1 maneuvers, pulse maneuvers and level deceleration maneuvers. Further, different lateral-directional maneuvers were performed including bank-to-bank maneuvers and rudder doublets. A full description of the maneuver characteristics is presented in [22]. The longitudinal maneuvers were executed by the elevators while the lateral-directional maneuvers were executed by the

ailerons, flaperons, and rudder. In order to identify the individual control effectiveness of ailerons and flaperons, four different control configurations were varied within the bank-to-bank maneuvers: execution of the maneuvers by 1) inner and outer ailerons, 2) only inner ailerons, 3) only outer ailerons, and 4) inner and outer flaperons. The maneuvers were ultimately repeated around different trim velocities in the range of $V_{TAS} = 18{-}30$m/s.

3 Flexible Aircraft Model

This section describes the flexible aircraft model. The modeling methodology is based on the framework of [4] and strip theory. The equations of motion are developed by representing the structural dynamics with free vibration modes and making use of the mean axis constraints. The aerodynamic strip forces and moments are modeled using a quasi-steady stability and control derivative approach.

3.1 Equations of Motion

The position $\boldsymbol{r}$ of an arbitrary mass element ρdV of an elastic body can be expressed in an inertial reference frame O_I (x_I, y_I, z_I) in terms of its relative position $\boldsymbol{p}$ to a body-reference frame O_{B^R} (x, y, z) and the position $\boldsymbol{r}_0$ of the origin of O_{B^R} (see Figure 4). The specified positions of the mass element in the inertial and body-reference frames are then related by the expression $\boldsymbol{r} = \boldsymbol{r}_0 + \boldsymbol{p}$. The body-reference axes O_{B^R} may rotate with an angular velocity $\boldsymbol{\omega}$ and their orientation may be defined by an arbitrary Euler angle sequence. The axes move with the body but are not necessarily attached to a material point.

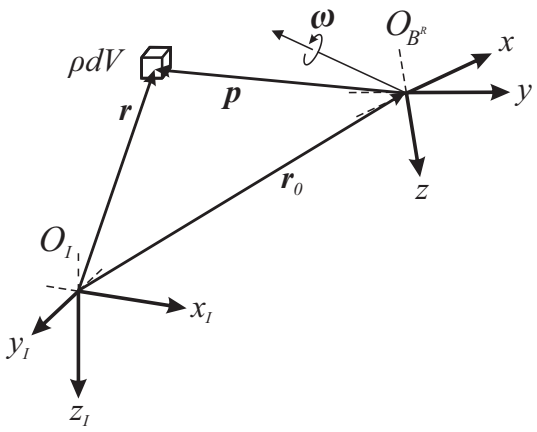

Fig. 4 Definition of a mass element's position using inertial O_I (x_I, y_I, z_I) and body O_{B^R} (x, y, z) reference frames

Assume that a modal description of the structure is available (e.g. from ground vibration tests and finite element model), such that the elastic deformation $\boldsymbol{d}$ at a point (x, y, z) can be expressed in terms of mode shapes $\Phi_j(x, y, z)$ and the generalized displacement coordinates $\eta_j(t)$ by

$$\boldsymbol{d}(x, y, z, t) = \sum_{j=1}^{n_e} \Phi_j(x, y, z)\eta_j(t) \tag{1}$$

where n_e denotes the number of elastic modes of the unconstrained, undamped vibration problem. Then, the position of the mass element relative to O_{B^R} can be separated into its undeformed part $\boldsymbol{s}(x, y, z)$ (rigid-body) and its deformation part $\boldsymbol{d}(x, y, z, t)$. The body-reference frame O_{B^R} may be used to develop the equations of motion of the unconstrained elastic body, assuming that each mass element is treated as a point mass. When doing so, inertial coupling can occur between the rigid degrees of freedom and the elastic degrees of freedom. However, it is found that with a suitable choice of O_{B^R} satisfying the mean axis constraints and the origin of O_{B^R} to be located at the instantaneous center of mass, the inertial coupling can be neglected [4, 25].

The mean axis, first introduced by [26], define a body frame for which the relative translational and angular momenta, due to the elastic deformation, are zero for all time $t \geq 0$. Combined with the modal description of the structure and only assuming small deformations (i.e. deformation and deformation rate are colinear), the constraints can be expressed by [4, 5]

$$\sum_{j=1}^{n_e} \frac{d\eta_j}{dt} \int_V \Phi_j \rho \, dV = 0, \qquad \sum_{j=1}^{n_e} \frac{d\eta_j}{dt} \int_V \boldsymbol{s} \times \Phi_j \rho \, dV = 0 \tag{2}$$

It can be shown that for the constraints to be satisfied, the elastic degrees of freedom require to be orthogonal to the translational and rotational rigid-body degrees of freedom, respectively [4, 27]. These conditions are guaranteed when the elastic deformations are represented by free vibration modes and the body-reference axes O_{B^R} are located at the instantaneous center of mass. The decoupled equations of motion of the elastic body are then given by [4, 11]

$$\dot{\boldsymbol{V}}|_{B^R} = -\boldsymbol{\omega}|_{B^R} \times \boldsymbol{V}|_{B^R} + \boldsymbol{T}_{B^R I}\boldsymbol{G}|_I + \frac{1}{m}\boldsymbol{F}^{ext}|_{B^R} \tag{3}$$

$$\dot{\boldsymbol{\omega}}|_{B^R} = -\boldsymbol{J}^{-1}(\boldsymbol{\omega}|_{B^R} \times (\boldsymbol{J}\boldsymbol{\omega}|_{B^R})) + \boldsymbol{J}^{-1}\boldsymbol{M}^{ext}|_{B^R} \tag{4}$$

$$\ddot{\eta}_j = -2\xi_j\omega_{n,j}\dot{\eta}_j - \omega_{n,j}^2\eta_j + \frac{1}{\mu_j}Q_{\eta_j} \tag{5}$$

The first two equations are formally equivalent to the standard nonlinear rigid-body flight dynamic equations for the translational and rotational degrees of freedom. Within these equations, $\boldsymbol{V}|_{B^R}$ and $\boldsymbol{\omega}|_{B^R}$ denote the linear and angular velocity vectors of the body-reference axes O_{B^R} with respect to the inertial reference axes O_I, expressed in body-reference coordinates. The gravity acceleration vector $\boldsymbol{G}|_I$ is expressed in O_I coordinates and transformed to O_{B^R} with the transformation matrix $\boldsymbol{T}_{B^R I}$. The aircraft mass is m and the inertial tensor J. Note that with the assumption of small deformations, J is considered constant. The vectors $\boldsymbol{F}^{ext}|_{B^R}$ and $\boldsymbol{M}^{ext}|_{B^R}$ denote the sum of external forces and moments expressed in coordinates of O_{B^R}. Only aerodynamic forces are considered in this work. The last Equation 5 represents the n_e linear differential equations for the structural dynamics in generalized coordinates. Within these equations, η_j denotes the generalized displacement, $\omega_{n,j}$ the undamped natural frequency, ξ_j the modal damping ratio, μ_j the generalized mass, and Q_{η_j} the generalized forces of each mode. Given the nonlinear rigid-body equations of motion and the linear equations of motion of the structure decoupled as presented, a coupling is solely due to $\boldsymbol{F}^{ext}|_{B^R}$, $\boldsymbol{M}^{ext}|_{B^R}$, and Q_{η_j}.

3.2 Quasi-Steady Strip Aerodynamics

The aerodynamic forces and moments of the test aircraft are modeled by applying strip theory. All effective lifting surfaces, i.e. wings, horizontal tail, and vertical tail, are divided into a finite number of spanwise strips. Each strip is then treated as a two-dimensional airfoil with its own geometric and aerodynamic characteristics. The aerodynamic characteristics are modeled by means of quasi-steady parameters. This implies that the resultant aerodynamic forces and moments at every time instant have reached their steady state values and are only dependent on the instantaneous configuration and local relative flow. The aerodynamic forces and moments of the fuselage are expressed by additional quasi-steady parameters acting on the center of mass.

Consider the aircraft with its lifting surfaces divided into a finite number of n_s spanwise strips, each with local width $\mathrm{d}y_i$, local chord c_i, and local surface area S_i. Each strip is assigned a structure support point (SP) at its centerline for which the instantaneous deformation (elastic translational displacement and elastic angular rotation) is known from the superposition of structural mode shapes and generalized displacements coordinates. The aircraft can then be treated as a discrete structure of interconnected points, as shown in Figure 5, which mark the elastic axes of the lifting surfaces.
For the modeling of aerodynamic forces and moments, each strip is further assigned two aerodynamic control points along its centerline, i.e. a neutral point (NP) which is assumed at the 25%-chord position and a zero pressure point (PP0) which is assumed at the 50%-chord position. In strip theory, the strips themselves are assumed non-deformable. Therefore, their motion can be described similar to the motion of a flat plate, as indicated in Figure 5 for the i-th strip.
The instantaneous position of each strip's structure support point, neutral point, and zero pressure point can be described relative to a global body-fixed frame O_{BG}. The frame O_{BG} is aligned with the body-reference axes O_{B^R} (origin at the center of mass) but is translated by a vector $\boldsymbol{b}_{cm}$, considered constant due

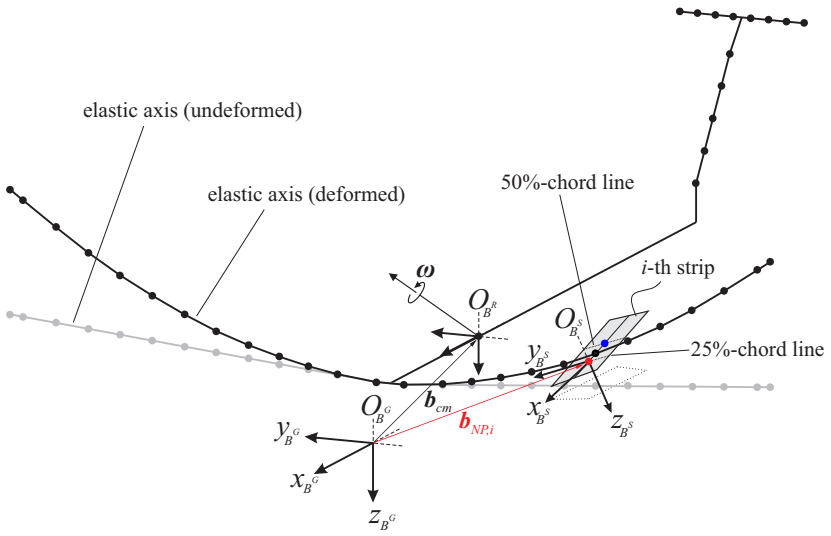

Fig. 5 Position and orientation of the i-th strip relative to the global body-fixed frame O_{B^G} and definition of the local strip-fixed frame O_{B^S}

to the assumption of small deformations [5]. Further, a local strip-fixed frame O_{B^S} is introduced which defines the instantaneous translation and orientation of the strip's 25%-chord line. Its origin is located at the neutral point and its orientation relative to O_{B^G} is defined by three rotations. These three rotations are the rigid and elastic dihedral angles ($\nu_{0,i}$, $\nu_{e,i}$), the rigid and elastic twist angles ($\varepsilon_{0,i}$, $\varepsilon_{e,i}$), and the rigid and elastic sweep angles ($\varphi_{25c,i}$, $\varphi_{e,i}$). The rotation from O_{B^G} to O_{B^S} is given by the transformation matrix $T_{B^S B^G}$. With the alignment of O_{B^G} and O_{B^R}, the transformation matrix $T_{B^S B^G}$ equals $T_{B^S B^R}$.
Let $\boldsymbol{b}_{NP,i}$ denote the instantaneous position of the strip's neutral point relative to the global body-fixed axes O_{B^G}. Further define $\boldsymbol{b}_{r,NP,i}$ as the rigid-body part of the position vector and

$$\boldsymbol{d}(x_i, y_i, z_i, t) = \sum_{j=1}^{n_e} \Phi_{d,j}(x_i, y_i, z_i)\eta_j(t) \tag{6}$$

$$\boldsymbol{\varphi}(x_i, y_i, z_i, t) = \sum_{j=1}^{n_e} \Phi_{\varphi,j}(x_i, y_i, z_i)\eta_j(t) \tag{7}$$

as the elastic translational displacement and elastic angular rotation vectors of the i-th structure support point along and about the body-reference axes, respectively. Then, under the assumption of no strip deformation, the position $\boldsymbol{b}_{NP,i}$ relative to the body-fixed axes O_{B^G} is calculated by

$$\boldsymbol{b}_{NP,i}(t) = \boldsymbol{b}_{r,NP,i} + \boldsymbol{d}(x_i, y_i, z_i, t) + T_{\varphi,i}(t)(\boldsymbol{b}_{r,NP,i} - \boldsymbol{b}_{r,SP,i}) \tag{8}$$

with $\boldsymbol{b}_{r,SP,i}$ denoting the rigid-body position vector of the i-th strip structure support point and $T_{\varphi,i}$ denoting the transformation matrix only due to elastic angular rotations in Equation 7. Note that $\boldsymbol{b}_{NP,i}$ is indicated time varying to distinguish between the non time varying terms in the equation. This notation is omitted for simplification in the following. Similar expressions can be derived for the position vectors of structure support point and zero pressure point.
The aerodynamic characteristics of the strips are modeled with quasi-steady parameters. In this sense, each strip is assigned a local non-dimensional lift coefficient and a local non-dimensional drag coefficient, where each coefficient itself is formed by stability and control derivatives normalized by S_i/S_{ref}

$$C_{L,i} = C_{L_0,i} + C_{L_\alpha,\varphi=0,i} \cdot \left(\frac{1+\sqrt{X_{0,i}}}{2} \right) \cdot \alpha_{\text{eff},i} + \sum_{n=1}^{n_c} C_{L_{\delta_{c,n}},i} \cdot \delta_{c,n} \tag{9}$$

$$C_{D,i} = C_{D_0,i} + k_i \cdot C_{L,i}^2 \tag{10}$$

In the equations, $C_{L_\alpha,\varphi=0,i}$ indicates the lift curve slope of the unswept strip, $\alpha_{\text{eff},i}$ is the strip's local effective angle of attack, and δ_c are the n_c deflections of the available control surfaces. Quasi-steady stall effects are included in terms of Kirchhoff's theory of flow-separation and an approximation of the steady flow-separation point $X_{0,i}$ based on hyperbolic-tangent [24]. For vertical stabilizer strips the non-dimensional lift coefficient is interpreted as a side force coefficient $C_{Y,i}$ with the effective angle $\beta_{\text{eff},i}$. All terms are assumed to act on the strip's neutral point, except for $C_{L_0,i}$ and $C_{L_{\delta_{c,n}},i} \cdot \delta_{c,n}$, which are assumed to act on the strip's zero pressure point and a variable point along the centerline as a function of the deflection [28], respectively. They are ultimately transferred to the strip's neutral point. The moments caused thereby are expressed in terms of non-dimensional moment coefficients $C_{l,i}$ (roll), $C_{m,i}$ (pitch), and $C_{n,i}$ (yaw). Non-dimensionality is achieved through dividing the moments by $\bar{s}$ (roll, yaw) and $\bar{c}$ (pitch), respectively. Lastly, the aerodynamic characteristics of the fuselage are modeled by additional non-dimensional force and moment coefficients with classical 1-point stability derivatives.
To calculate the effective angles in Equation 9, the local relative flow at each strip has to be determined. This is achieved by summing all individual flow components at O_{B^S}, i.e. the linear aerodynamic velocity of O_{B^R}, plus additional terms due to rotation about O_{B^R}, and the velocity of the structure:

$$\boldsymbol{V}_{A,i}|_{B^R} = \boldsymbol{V}_A|_{B^R} + \boldsymbol{\omega}_A|_{B^R} \times (\boldsymbol{b}_{NP,i} - \boldsymbol{b}_{cm}) + \sum_{j=1}^{n_e} \Phi_{d,j}(x_i, y_i, z_i)\dot{\eta}_j \tag{11}$$

The induced velocity due to elastic rotation about the structure support point is neglected. In Equation 11, $\boldsymbol{V}_A|_{B^R}$ and $\boldsymbol{\omega}_A|_{B^R}$ denote the linear and angular aerodynamic velocity vector at O_{B^R}, respectively. Downwash effects are taken into account at tailplane strips by the induced downwash angle $\varepsilon_{T,i}$. It is proportional to the angle of attack at O_{B^R} and flaperon deflections, delayed by the time $\Delta t_{\varepsilon_T,i}$ the flow requires to reach the tailplane strips [29].

$$\varepsilon_{T,i}(t) = \frac{\partial \varepsilon_T}{\partial \alpha} \cdot \alpha(t - \Delta t_{\varepsilon_T,i}) + \sum_{n=1}^{n_f} \frac{\partial \varepsilon_T}{\partial \delta_{f,n}} \cdot \delta_{f,n}(t - \Delta t_{\varepsilon_T,i}) \tag{12}$$

Herein, $\partial\varepsilon_T/\partial\alpha$ and $\partial\varepsilon_T/\partial\delta_{f,n}$ denote the partial derivatives of the downwash angle to the angle of attack at O_{B^R} and n_f flaperon deflections. In this work, the calculation of $\Delta t_{\varepsilon_T,i}$ is simplified by taking the mean distance between wing and horizontal or vertical tail strip neutral points along x_{B^R}, divided by the airspeed V_A at O_{B^R}. The downwash angles are then used to correct the local relative flow at the tailplane strips. The local relative flow is originally defined in the local strip aerodynamic frame O_{A^S}, but as given in Equation 11, is already expressed in components along O_{B^R}. Then, the angles α_i and β_i define the orientation of O_{A^S} relative to O_{B^R}. The local relative flow at the i-th strip is illustrated in Figure 6.
With transformation matrix $T_{B^S B^R}$, the local relative flow from Equation 11 can be expressed in O_{B^S} coordinates. It is then straight forward to calculate the effective angles needed for the calculation of the aerodynamic force coefficient in Equation 9, by

$$\alpha_{\text{eff},i} = \arctan\left(\frac{w_{A,i}|_{B^S}}{u_{A,i}|_{B^S}}\right), \qquad \beta_{\text{eff},i} = \arcsin\left(\frac{v_{A,i}|_{B^S}}{|\boldsymbol{V}_{A,i}|}\right) \tag{13}$$

Indicated in Figure 6, the orientation of the force and moment coefficients is either given along the coordinates of O_{A^S} (defined by α_i and β_i) or along the normal flow component $\boldsymbol{V}_{N,i}$, but overall rotated about the body-reference axis x_{B^R} by the rigid and elastic dihedral angle[1]. They can be expressed in components of the body-reference axes O_{B^R} through a sequence of rotations involving these angles and summarized to coefficient vectors $\boldsymbol{C}_i^F|_{B^R}$ and $\boldsymbol{C}_i^M|_{B^R}$, respectively. The resulting forces and moments at

[1] Assuming no elastic sweep angle $\varphi_{e,i} = 0$. If $\varphi_{e,i} \neq 0$, a further rotation is given by this angle.

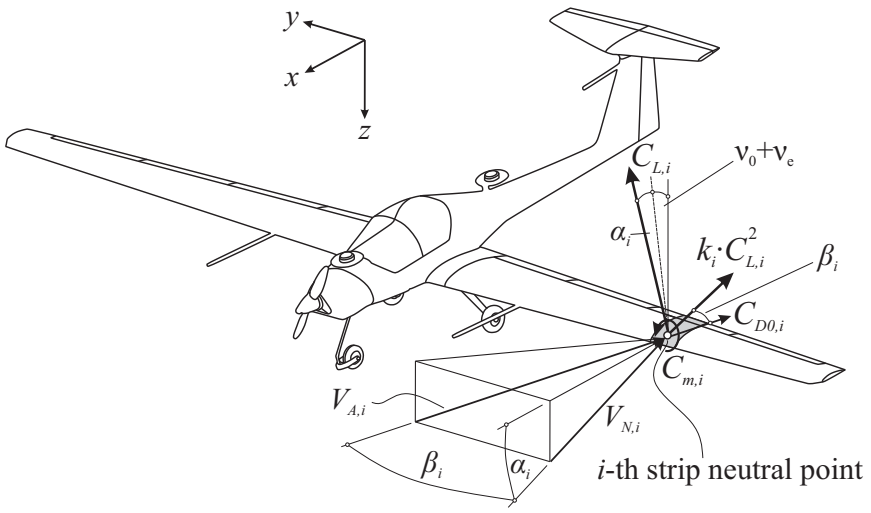

Fig. 6 Local relative flow at the i-th strip and force and moment coefficients (assuming $\varphi_{e,i} = 0$)

either the neutral point (strips) or the center of mass (fuselage) are then given by

$$\boldsymbol{F}_i^A|_{B^R} = \overline{q}_{N,i} S_{\text{ref}} \boldsymbol{C}_i^F|_{B^R} \tag{14}$$

$$\boldsymbol{M}_i^A|_{B^R} = \overline{q}_{N,i} S_{\text{ref}} \boldsymbol{D}\, \boldsymbol{C}_i^M|_{B^R} \tag{15}$$

with the diagonal matrix $\boldsymbol{D}$, which has the main diagonal elements $\{\overline{s}, \overline{c}, \overline{s}\}$, and the effective dynamic pressures for wing and horizontal tail strips (Equation 16a) and vertical tail strips (Equation 16b) as

$$\overline{q}_{N,i} = \overline{q}_{A,i} \cos^2(\beta_{\text{eff},i}) \tag{16a}$$

$$\overline{q}_{N,i} = \overline{q}_{A,i} \cos^2(\alpha_{\text{eff},i}) \tag{16b}$$

The forces and moments are ultimately transferred to the center of mass and summed up for the equations of motion of the rigid-body degrees of freedom. The generalized forces Q_{η_j} for the equations of the structural dynamics can be obtained by first transferring all strip forces and moments to their respective structure support points. Then, the resulting strip forces and moments are collected in vector form and are subsequently transformed with the transposed mode shapes

$$Q_{\eta_j} = \Phi_j^T \begin{pmatrix} \boldsymbol{F}_{x,SP}^A & \boldsymbol{F}_{y,SP}^A & \boldsymbol{F}_{z,SP}^A & \boldsymbol{M}_{x,SP}^A & \boldsymbol{M}_{y,SP}^A & \boldsymbol{M}_{z,SP}^A \end{pmatrix}^T \tag{17}$$

4 Flexible Model Identification and Evaluation

This section is concerned with the identification of the flexible aircraft model and the evaluation of the results. Prior to the actual parameter estimation, a simulation model is assembled and implemented in MATLAB/SIMULINK. Given the equations of motion of the flexible aircraft and the quasi-steady strip aerodynamics model, the model is combined with additional models from the in-house library FLYSIM. These include an earth and atmosphere model, a wind and turbulence model, and an actuator model for the representation of servo and control surface dynamics. Moreover, a propulsion model and landing gear model are added. Subsequently, a suitable set of maneuvers is selected. This is accomplished by post-processing the gathered flight test data and transferring all the available measurement parameters listed in Table 1 to the center of gravity. Moreover, the load measurement parameters are corrected by the dead weight of the structure. The selection of maneuvers is based on different criteria such as precision of maneuver execution, dynamic pressure variations, and atmospheric disturbance.

4.1 Parameter Estimation

The estimation of model parameters is performed with the in-house tool DAVIS, using the output error method in the time domain and maximum likelihood estimation [24]. Suitable model parameters Θ_i to be estimated are required. Since the structural dynamics model was identified from GVT data, only parameters of the strip aerodynamics model are estimated. Initial distributions of the normalized stability and control derivatives are obtained from vortex-lattice-method calculations of the aircraft in the open source software tool XFLR5. The aircraft is modeled without fuselage as advised by XFLR5. To this end, all lifting surfaces are divided into spanwise strips based on geometric properties and the resolution of local flow effects. A total number of 48 wing strips, 8 horizontal tail strips, and 5 vertical tail strips are considered. Subsequently, the locations of the strips are used to define associated structure support points as described in subsection 3.2 and determine the structural mode shapes from the adapted FE-model. The resulting distributions are shown in Figure 7.

According to the aerodynamic parametrization of the non-dimensional force coefficients, separate distributions are obtained for zero coefficients, stability derivatives, and control derivatives. The associated control surface deflections are $\delta_{a,\text{in}}$ and $\delta_{a,\text{out}}$ for inner and outer ailerons, $\delta_{f,\text{in}}$ and $\delta_{f,\text{out}}$ for inner and outer flaperons, δ_r for the rudder, and δ_e for the elevators. Each wing control surface is assumed to only influence the lift on the side of the wing it is attached to. Parameters for linearly scaling the initial distributions are introduced and defined as estimation parameters. In this way, the initial distributions can be adapted in the estimation process with a limited number of estimation parameters. On the other hand, the achievable solution is constrained by the qualitative shapes of the initial distributions. Separate scaling parameters are defined for each lifting surface, i.e. wings, horizontal tail, and vertical tail. Scaling parameters for the control derivative distributions of opposite control surfaces are either paired or grouped based on the control allocations used in the flight tests (indicated in Figure 7 with the color code). The additional stability derivatives of the fuselage and downwash parameters are treated as direct estimation parameters with no effect on the distributions. Stall parameters are determined separately from flight data and kept fixed for the estimation. Measurement outputs of the rigid-body motion are selected and set as criteria for the parameter estimation:

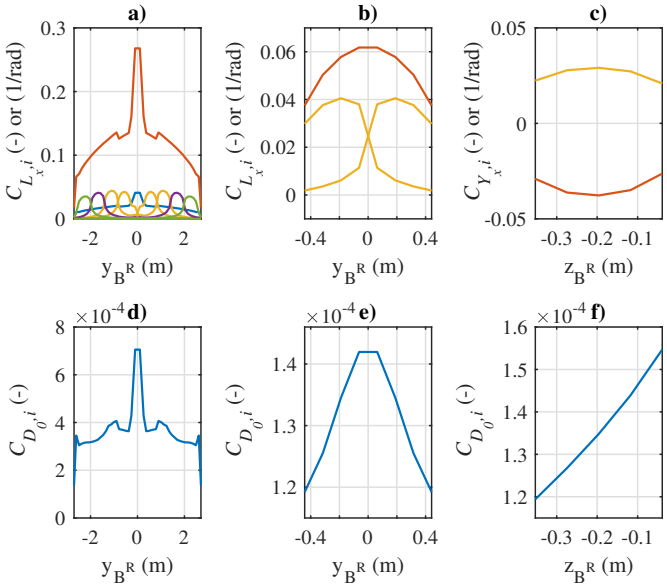

Fig. 7 Initial derivative distributions from XFLR5: a) wing lift with $C_{L_0,i}$ (—), $C_{L_\alpha,i}$ (—), $C_{L_{\delta_f},i}$ (—), $C_{L_{\delta_{a,\text{in}},i}}$ (—), $C_{L_{\delta_{a,\text{out}},i}}$ (—), b) horizontal tail lift with $C_{L_\alpha,i}$ (—), $C_{L_{\delta_e},i}$ (—), c) vertical tail side force with $C_{Y_\beta,i}$ (—), $C_{Y_{\delta_r},i}$ (—), d) to f) parasitic drag of wing, horizontal and vertical tail

$$y = \begin{bmatrix} V_{TAS} & \alpha & \beta & \dot{p} & \dot{q} & \dot{r} & p & q & r & \Phi & \Theta & \Psi & a_x & a_y & a_y & u & v & w \end{bmatrix} \tag{18}$$

The values and standard deviations of the final estimated distribution scaling parameters are listed in Table 3. Low standard deviations are achieved for all estimated parameters. A value close to 1 indicates an estimation result close to the initial distributions from XFLR5. This is found for the parameter $k\_C_{Y_\beta}$ of the vertical tail, the parameters $k\_C_{L_\alpha,\text{wing}}$ and $k\_C_{L_\alpha,\text{htp}}$ of the wing and the horizontal tail, and the parameter $k\_C_{L_{\delta_{a,\text{out}}}}$ of the outer ailerons. Least agreement with the initial distributions from XFLR5 are found for the parameters $k\_C_{D_0}$ of all lifting surfaces, $k\_C_{L_0,\text{wing}}$ of the wing, and $k\_C_{L_{\delta_e}}$ of the elevators.

The result of $k\_C_{D_0}$ being significantly underestimated by XFLR5 is expected considering the approximation of viscous drag from 2D polar data associated with the calculation method. Table 4 further lists the values and standard deviations of the final estimated additional parameters of the fuselage and downwash. Only few parameters for the most dominant fuselage effects are incorporated in the final parameter set. An increased standard deviation is only observed for the parameter $C_{Y_{\beta,\text{fuse}}}$ of the fuselage.
Matching plots of the identification result are shown in Figure 8 for longitudinal and lateral maneuvers. The plots up to the last four represent measurement parameters of the rigid-body motion. A good overall identification result is achieved for all maneuvers. Especially the fast aircraft dynamics are matched well, which is important for control law design. Very good matches are also achieved for the translational rigid-body accelerations (a_x, a_y, a_z), which are directly related to the external forces acting on the aircraft. Note that gravitational accelerations are not measured by the sensors. Some model deficiencies are found for the measurement parameters true airspeed V_{TAS} and pitch angle Θ, which indicate slight deviations of the model's pitching moment to the actual aircraft's pitching moment. Unexpected model behavior is also observed in the last part of the level deceleration maneuver. However, judging from the control action of ailerons and rudder, an undetected asymmetric atmospheric disturbance is suspected to influence the maneuver.

Table 3 Estimated scaling parameters

Θ_i	Value	Std. deviation
$k\_C_{D_0}$	3.1389	1.95%
$k\_C_{Y_\beta}$	0.9988	0.82%
$k\_C_{Y_{\delta_r}}$	0.8234	1.33%
$k\_C_{L_0,\text{wing}}$	0.3105	3.26%
$k\_C_{L_\alpha,\text{wing}}$	1.1425	0.87%
$k\_C_{L_\alpha,\text{htp}}$	0.8897	0.76%
$k\_C_{L_{\delta_f}}$	0.7746	1.09%
$k\_C_{L_{\delta_e}}$	0.5646	0.74%
$k\_C_{L_{\delta_{a,\text{in}}}}$	0.7401	1.08%
$k\_C_{L_{\delta_{a,\text{out}}}}$	0.9731	0.99%

Table 4 Estimated additional parameters

Θ_i	Value	Std. deviation
$\partial\varepsilon_T/\partial\alpha$	0.411	1.75%
$\partial\varepsilon_T/\partial\delta_f$	0.0248	1.72%
$C_{Y_{\beta,\text{fuse}}}$	-0.1295	11.82%
$C_{l_{0,\text{fuse}}}$	-0.0017	1.01%
$C_{m_{0,\text{fuse}}}$	-0.0378	4.87%

4.2 Evaluation

The identified model is further evaluated with regard to its capability to estimate distributed structural loads and its use in active load control law design. To this end, shear forces Q_z measured at middle and inner load measurement stations along the wing are compared to the model outputs in the last four plots of Figure 8. The outputs are constructed to only capture the aerodynamic loads of the deformed structure. This is achieved by summing all aerodynamic strip forces in z_{B^R}-direction up to the respective load measurement stations. Inertial loads are neglected such that an overestimation of shear forces is expected during dynamic peaks. Close matches are found for all shear forces for the majority of maneuvers. This result indicates an overall plausible representation of the actual aerodynamic force distribution along the wing. Moreover, the close match of shear forces at the inner load measurement stations LMS5 (left) and LMS6 (right) are in good agreement with the identification result of a_z, since both stations capture the majority of aerodynamic forces in z_{B^R}-direction. An unexpected model behavior is solely found for the inner load measurement stations during flaperon bank-to-bank maneuvers, where the effects of local load increase/decrease due to flaperon deflection and the resulting rotation of the aircraft are not represented correctly. It is suspected that the negligence of a dedicated fuselage model within XFLR5 and therewith negligence of wing-fuselage interaction effects on the initial derivative distributions is a cause of the deviation. Based on these results, the identified model is capable of computing realistic distributed aerodynamic forces and moments and thus is well suited for state of the art model-based load estimation techniques [30]. This aspect combined with the simple model structure also provides a suitable basis for real-time simulation and the design of active load control laws.

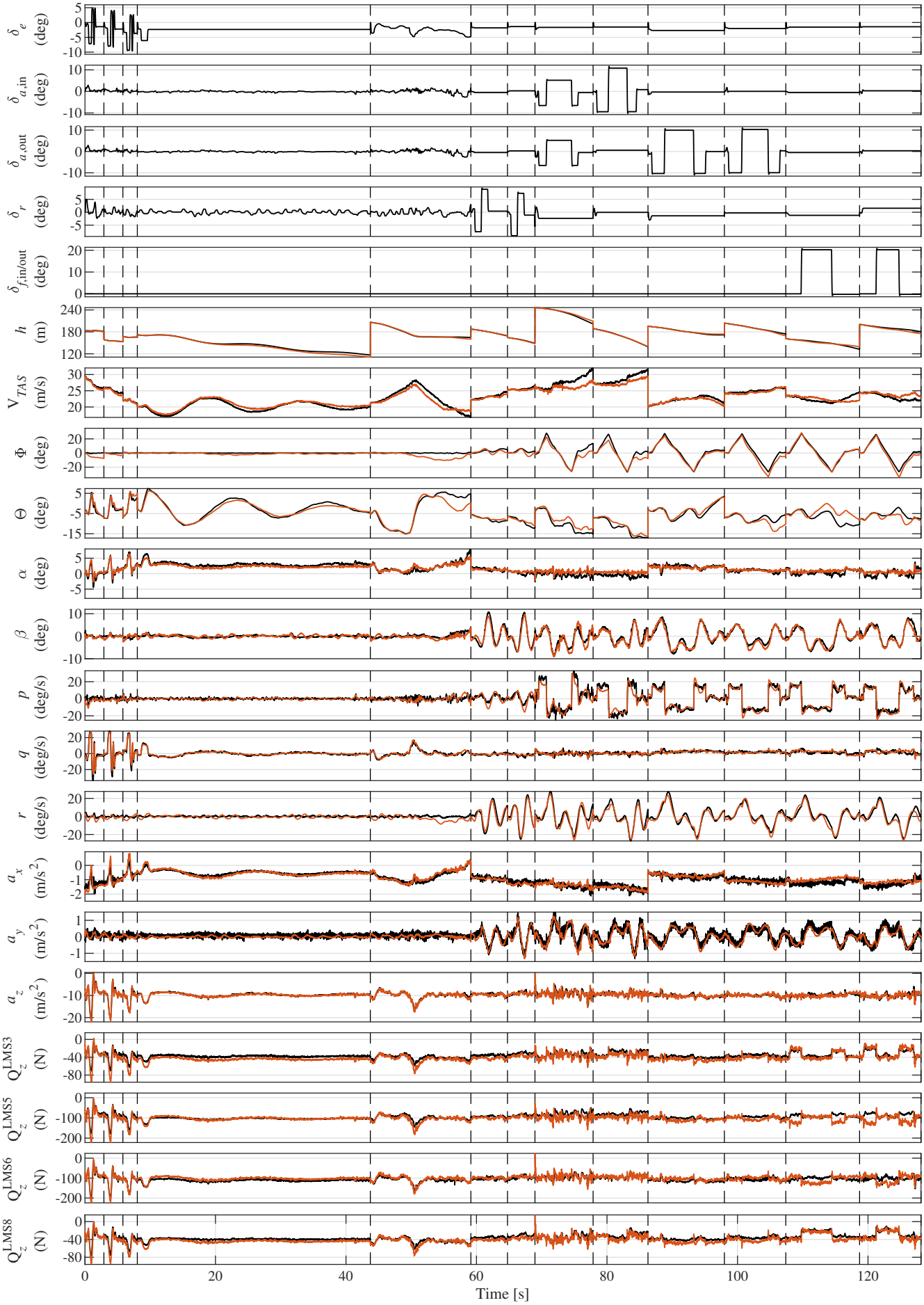

Fig. 8 Identification result for longitudinal/lateral maneuvers with measurement parameters of the rigid-body motion and distributed shear forces, measurement (—), simulation (—), maneuver separation (- -)

5 Conclusion

A control-oriented modeling framework for slightly flexible aircraft suitable for parameter identification in the time domain was presented. It combines linear structural dynamics and a distributed quasi-steady aerodynamics model using strip theory. The applicability of the modeling framework was demonstrated for a slightly flexible 25kg fixed-wing UAV. Free vibration modes and mode shapes of the structure were obtained from ground vibration tests. Initial distributions for the stability and control derivatives of the strip aerodynamics were derived from vortex-lattice-method steady-flow calculations. They were subsequently adapted based on flight test data using the output error method in the time domain and maximum likelihood estimation. The use of scaling parameters for adapting the initial distributions is demonstrated to be an efficient approach for achieving a limited number of estimation parameters. A good overall identification result and close match of the fast aircraft dynamics was achieved. Good agreements with the initial derivative distributions were found for the lift curve slope and angle of sideslip dependent stability derivative distributions, while viscous drag effects were significantly underestimated by the vortex-lattice-method calculations. Further, the evaluation of distributed shear force measurements along the wing demonstrated the capability of the model to compute realistic distributed aerodynamic forces and moments. The resultant computationally efficient model provides a suitable basis for real-time simulation, loads estimation, and active load control law design. The latter highly benefit from the capability of the strip aerodynamic model structure to yield distributed forces and moments. Possible future work includes the improvement of the derivative distributions based on high-fidelity numerical or experimental data.

Acknowledgments

The authors would like to acknowledge Lothar Desel and pilot Rasmus Köhler for their support during the flight test campaign. Special thanks is further devoted to Karsten Henning for his contribution to the results. This work was partly funded by the research project "Advanced load analysis and observer methods for innovative aircraft configurations" (ELASTIK), which is supported by the german Federal Ministry for Economic Affairs and Climate Action in the national LuFo V-3 program. Any opinions, findings and conclusions expressed in this document are those of the authors and do not necessarily reflect the views of the other project partners.

Supported by:

on the basis of a decision
by the German Bundestag

References

[1] Francois Kubica. New flight control laws for large capacity aircraft experimentation of airbus a 340. In *ICAS, Congress, 21st, Melbourne, Australia*, 1998.

[2] Ilhan Tuzcu and Leonard Meirovitch. Effects of flexibility on the stability of flying aircraft. *Journal of Dynamic Systems, Measurement, and Control*, 127(1):41–49, jun 2004. DOI: 10.1115/1.1870040.

[3] Ravindra Jategaonkar, Dietrich Fischenberg, and Wolfgang von Gruenhagen. Aerodynamic modeling and system identification from flight data-recent applications at DLR. 41(4):681–691, jul 2004. DOI: 10.2514/1.3165.

[4] Martin R. Waszak and David K. Schmidt. Flight dynamics of aeroelastic vehicles. 25(6):563–571, jun 1988. DOI: 10.2514/3.45623.

[5] David K. Schmidt and David L. Raney. Modeling and simulation of flexible flight vehicles. *Journal of Guidance, Control, and Dynamics*, 24(3):539–546, may 2001. DOI: 10.2514/2.4744.

[6] Kimberly Pete, Sonya Smith, and Dan Vicroy. Model validation for wake-vortex/aircraft encounters. American Institute of Aeronautics and Astronautics, aug 2000. DOI: 10.2514/6.2000-3979.

[7] AC De Bruin. S-wake assessment of wake vortex safety. *National Aerospace Laboratory NLR*, 2003.

[8] Dietrich Fischenberg. A method to validate wake vortex encounter models from flight test data. In *27th International Congress of the Aeronautical Sciences*. International Council of the Aeronautical Sciences Nice, France, 2010.

[9] Michael Selig. Modeling full-envelope aerodynamics of small UAVs in realtime. American Institute of Aeronautics and Astronautics, jun 2010. DOI: 10.2514/6.2010-7635.

[10] Flávio Silvestre and Pedro Paglione. Dynamics and control of a flexible aircraft. American Institute of Aeronautics and Astronautics, jun 2008. DOI: 10.2514/6.2008-6876.

[11] Flávio J. Silvestre and Robert Luckner. Experimental validation of a flight simulation model for slightly flexible aircraft. 53(12):3620–3636, dec 2015. DOI: 10.2514/1.j054023.

[12] Stuart Andrews. *Modelling and simulation of flexible aircraft : handling qualities with active load control*. PhD thesis, 2011.

[13] E. Carson Yates. Modified-strip-analysis method for predicting wing flutter at subsonic to hypersonic speeds. *Journal of Aircraft*, 3(1):25–29, jan 1966. DOI: 10.2514/3.43702.

[14] J. Weissinger. The lift distribution of swept-back wings. Technical Report NACA-TN-1120, National Advisory Committee for Aeronautics, 1947.

[15] Herbert Wagner. Über die Entstehung des dynamischen Auftriebes von Tragflügeln. *ZAMM - Zeitschrift für Angewandte Mathematik und Mechanik*, 5(1):17–35, 1925. DOI: 10.1002/zamm.19250050103.

[16] J. Gordon Leishman. Unsteady lift of a flapped airfoil by indicial concepts. *Journal of Aircraft*, 31(2):288–297, mar 1994. DOI: 10.2514/3.46486.

[17] Bruno Giordano de Oliveira Silva. Data gathering and preliminary results of the system identification of a flexible aircraft model. American Institute of Aeronautics and Astronautics, jun 2011. DOI: 10.2514/6.2011-6355.

[18] Bruno Giordano de Oliveira Silva and Wulf Moennich. System identification of flexible aircraft in time domain. American Institute of Aeronautics and Astronautics, aug 2012. DOI: 10.2514/6.2012-4412.

[19] Christophe Le Garrec and François Kubica. In-flight structural modes identification for comfort improvement by flight control laws. 42(1):90–92, jan 2005. DOI: 10.2514/1.3733.

[20] C Niemann, M Montel, and F Thielecke. Development of an air data system for an unmanned research aircraft. In *Deutscher Luft-und Raumfahrtkongress*, 2014.

[21] Karsten Henning, Mike Montel, and Frank Thielecke. Experimentelle Ermittlung der modalen Strukturparameter eines skalierten Flugversuchstraegers mittels Low-Cost Sensoren. In *Deutscher Luft- und Raumfahrtkongress DLRK*, Muenchen, Germany, 2017.

[22] Matthias Krings, Karsten Henning, and Frank Thielecke. Flight test oriented autopilot design for improved aerodynamic parameter identification. In *Advances in Aerospace Guidance, Navigation and Control*, pages 265–276. Springer Berlin Heidelberg, 2013.

[23] Matthias Krings, Bjoern Annighoefer, and Frank Thielecke. Ultra - unmanned low-cost testing research aircraft. In *American Control Conference ACC*, 2013.

[24] Ravindra Jategaonkar. *Flight vehicle system identification : a time domain methodology*. American Institute of Aeronautics and Astronautics, Reston, Va, 2006.

[25] Sally Ann Keyes, Peter Seiler, and David K. Schmidt. Newtonian development of the mean-axis reference frame for flexible aircraft. *Journal of Aircraft*, 56(1):392–397, jan 2019. DOI: 10.2514/1.c035041.

[26] Ronald Douglas Milne. Dynamics of the deformable aeroplane. Technical report, Aeronautical Research Council London (United Kingdom), 1964.

[27] J.R. Canavin and P.W. Likins. Floating reference frames for flexible spacecraft. *Journal of Spacecraft and Rockets*, 14(12):724–732, dec 1977. DOI: 10.2514/3.57256.

[28] H. Schlichting and E. Truckenbrodt. *Aerodynamik des Flugzeuges: Zweiter Band*. Springer Berlin Heidelberg, 1960. DOI: 10.1007/978-3-642-53046-3.

[29] Rudolf Brockhaus, Wolfgang Alles, and Robert Luckner. *Flugregelung*. Springer Berlin Heidelberg, 2011. DOI: 10.1007/978-3-642-01443-7.

[30] Mike Montel and Frank Thielecke. Validation of a hybrid observer method for flight loads estimation. In *31st Congress of the International Council of the Aeronautical Sciences ICAS*, Belo Horizonte, Brasil, September 2018. International Council of the Aeronautical Sciences (ICAS).